International Journal on Advanced Science Engineering Information Technology

Vol.12 (2022) No. 4
ISSN: 2088-5334

Scalar Damage Modeling of Reinforced Concrete Beam Under Polarized Monotonic Stress Field Using Ultrasonic Pulses

Gabriel I. Gamana [a,*], Melito A. Baccay [a]

[a] *Department of Civil Engineering, Technological University of the Philippines, Ayala Blvd, Ermita, Manila, 1000, Philippines*
Corresponding author: [*]gabriel_gamana@tup.edu.ph

Abstract **— The extensive use of concrete has increased the demand for reliable non-destructive evaluation (NDE) techniques to investigate aging structures thoroughly. Among these NDE techniques, the ultrasonic pulse velocity (UPV) test stands out because of its versatility in-field application and its relatively low cost. Unfortunately, despite the promising results of UPV and pulse attenuation, its dependency on the nature of the applied stress is continuously overlooked. This research pioneered an approach that focused on developing a scalar damage model that relates the damage variable to the nature and the intensity of the applied stresses, concrete strength, and steel ratio. The results showed that transducers placed at different locations exhibited different deterioration rates of which the higher the applied stress intensity, the higher the scalar damage's inclination angle. Transducers placed in concrete under compression stress deteriorate earlier as compared to concrete under tension. As the steel ratio and concrete strength increase, the inclination angle of the elastic data trend also decreases. It was established in this research that beams with ductile response to the applied load tend to have a larger inclination angle for the elastic data trend while its UPV readings at the data trend's transition are greater than 3000 m/s which is conventionally accepted as concrete within normal to good quality although the beam undergoes critical stress redistribution as it approaches plastic hinging. Ultimately, this study showed that the scalar damage model exhibited superiority in quantitatively monitoring early damage propagation, in contrast to UPV reading and pulse attenuation.**

Keywords **— Scalar damage; ultrasonic pulses; damage mechanics; microcracks; elastic modulus.**

Manuscript received 22 Oct. 2021; revised 25 Dec. 2021; accepted 17 Jan. 2022. Date of publication 31 Aug. 2022.

I. INTRODUCTION

Concrete has become one of the icons of economic development since construction played a significant role in providing higher living standards; it changed how we live, work, and travel. The United Nations (UN) estimates that in 1950 around 30% of the world's population was urbanized, while in 2018, just over a half with 55%, and by 2050, around 68% will live in urbanized areas [1]. On the other hand, the International Monetary Fund (IMF) projected that global economic growth would be 5.9 percent in 2021 and 4.9 percent in 2022, considering the current pandemic's effects [2]. This great news potentially excites the global construction industry since the construction sector has a strong economic development connection. Additional medical infrastructures, such as hospitals and quarantine facilities need to be constructed to boost the response whenever the pandemic re-intensify.

Moreover, when the global Gross Domestic Product (GDP) growth rate rises above moderate after overcoming the effect of the pandemic, the construction activities expand in a higher proportion. Likewise, GDP is proportional to infrastructure spending, which means more investment in infrastructure allows the country to increase its production capacity, which will lead to a higher GDP growth rate [3]**.** There is no doubt that the construction industry is one of the promising markets worldwide.

However, besides the increases in the number of shares, stocks, and GDP, these values only mean more social and economic infrastructure projects are to be constructed. Investing in infrastructure means investing in a long-term solution since a developing country requires more infrastructure to support its constituent's growing demands. To ensure that these infrastructures will have a reasonable rate of return, they must efficiently perform their functions within their designed life span. In order to do that, a maintenance routine is a must to address the material's deterioration in the early stage before they become irreversible damage.

On the other hand, extensive use of concrete has increased the demand for reliable non-destructive evaluation (NDE) techniques to investigate aging structures thoroughly [4].

Unfortunately, visual inspection is the most common practice in some developing countries to monitor the concrete's structural integrity. The problem is that it is fully experienced-based, applicable only when the damage is visible and subjective, or non-quantitative [5]. Accurate structural integrity monitoring is critical since natural disasters such as Super Typhoons and Earthquakes are always a significant threat.

As technology advances, the systematic implementation of damage detection and characterization strategy for engineering structures paved the way for developing the so-called Structural Health Monitoring (SHM). Part of this system uses NDE techniques for accurate quantitative measurement of structure components' mechanical damage [6]. Moreover, numerous NDE techniques have been developed for civil engineering applications, such as rebound hammer, ultrasonic pulse velocity test, nonlinear ultrasonic test, acoustic emission, digital image correlation, and aerial drone technology. Among these NDE techniques, the ultrasonic pulse velocity (UPV) test stands out because of its versatility in the in-situ application and its relatively low cost [4].

A. Ultrasonic Pulses

UPV test is used to assess the quality of concrete by passing a pulse of longitudinal vibration created by the electro-acoustical transducer held in contact with the concrete surface. The generated pulse undergoes multiple reflections, and a complex system of stress waves was developed, such as longitudinal and shear waves that propagate through the concrete. A second transducer receives the wave and converted it into an electrical signal used to produce the pulse's transit time to be measured [7]. This transit time determines the velocity of ultrasonic pulses, which is one of the three aspects of ultrasound other than frequency and amplitude. Moreover, UPV delivers information about different characteristics of the propagating medium since results from the infinitesimal isotropic linearly elastic materials can directly relate ultrasonic longitudinal (P wave) and shear wave (S wave) velocities to the density, Poisson's ratio, and elastic modulus of the propagating medium [4]. Furthermore, UPV reading is just one of the two aspects of the linear ultrasonic test. The second aspect is pulse attenuation, the process by which the Peak-to-Peak amplitude of the ultrasonic pulses decreases concerning damage propagation.

The earliest study that used sound wave's vibrational motion to determine the material's mechanical properties under laboratory conditions was conducted by Powers [8] in 1938. More than ten years later, in 1948, the development of ultrasonic waves began when Jones [9] published his paper about applying ultrasonic waves to concrete materials, followed by the publication of Leslie and Chessman [10] in 1949 that used ultrasonic waves to study the deterioration and cracks of concrete. They worked independently to develop the now so-called Ultrasonic Pulse Velocity (UPV) test [11]. Shah and Chandra [12], in 1970 extended the application of ultrasonic waves by introducing variations in ultrasonic transducers with different resonant frequencies, such as 25, 250, 750, and 2250 kHz, as well as the variations on the applied loads, such as sustained, monotonically increasing, and cyclic compression loads. The result showed that both the UPV and pulse attenuation were correlated to microcrack growth, and the authors also concluded that increasing the resonant frequencies of the transducers also increased the sensitivity to microcrack growth [12]. Unfortunately, despite the promising results of UPV and pulse attenuation, its dependency on the nature of applied stress is continuously overlooked. Moreover, Suaris and Fernando in 1987 showed that the pulse attenuation or the Peak-to-Peak amplitude starts to decrease as the load reaches 40 percent of the ultimate capacity [13]. The authors also concluded that pulse attenuation is more sensitive in microcrack growth detection than ultrasonic pulse velocity [14].

Meanwhile, Nagy in 1998 emphasized that linear acoustic characteristics, such as UPV and attenuation, are not sensitive enough to detect microscopic imperfection due to early fatigue damage that serves as the nuclei of fracture since the nuclei are smaller than the acoustic wavelength [15]. The author added that early fatigue damage could manifest into excess in ultrasonic nonlinearity that can characterize fatigue damage. This characterization can be done by first considering the acoustoelastic effect, which is the dependency of the UPV to the applied stress, and secondly is the spectral frequency analysis or the so-called harmonic generation [16]. Since then, various studies such as Zheng et al. [17] in 1999 and Van Den Abeele et al. [18] in 2001 consistently highlighted that nonlinear acoustic wave is far more sensitive to damage detection caused by fatigue stress than linear acoustic waves [19]. Meanwhile, numerous studies, such as Yoo et al. [20], Ju et al. [21], and Camara [22], showed that the linear UPV test is consistent in quantitatively monitoring the strength of self-healing and high-strength concrete. Simultaneously, several studies, such as Lillamand et al. [23], Nogueira et al. [4], and Nogueira et al. [24], also conducted studies on concrete under stress and showed that the effect of third-order elastic variables could be used to enhance the sensitivity of linear UPV test to detect microscopic damage.

Moreover, the latest trends in ultrasonic wave studies, such as Chen et al. [25] and Ongpeng et al. [26], both conducted in 2018, incorporated Artificial Neural Network (ANN), a computer algorithm capable of modeling a nonlinear system in concrete under applied stresses. ANN is a data mining tool that serves as a brain with a neural structure that can learn from its own data set. ANN can improve our data interpretation and predict future studies' possible outcomes. Furthermore, this research focused on linear acoustics, considering both the UPV, specifically the longitudinal wave and pulse attenuation, and studying its effects concerning the RC beam's steel ratio, concrete strength, nature, and intensity of the applied stresses.

B. Microcrack

Microcracks are internal cracks responsible for developing the nonlinear stress-strain curve of concrete under uniaxial monotonic compressive loading. Microcracks are classified in two different forms; first, microscopic cracks that occur within aggregates and cement paste interface are called bond cracks. Secondly, microscopic cracks that are formed within the mortar between the aggregates are called mortar cracks [27]. The study of concrete progressive failure began in 1928 when Richart et al. [28] published their observation about the

volumetric change of concrete when the applied stress reaches 75 to 85 percent of the concrete strength; the authors classified this level of the loads as the critical level. In 1948 two decades after Jones used UPV to study the fracture of concrete and concluded that crack formation starts around 25 to 30 percent of concrete capacity [9], while the subsequent studies using UPV, such as L'Hermite [29] in 1954, Rusch [30] in 1959, and Sell [31] at the same year presents in detail the crack propagation between 50 to 75 percent of the concrete capacity.

On the other hand, Hsu et al. [32] and Slate & Olsefski [33] in 1963 cut open the concrete cylinders and investigated microcrack propagation using a microscope and X-ray. These authors concluded that microcracks development is related to the nonlinear behavior of concrete in the stress-strain curve. At the same time, Newman [34] in 1968 pointed out that the 75 percent level of the concrete capacity is the discontinuity stress level that signals the end of concrete quasi-elastic behavior [35].

Wight and MacGregor consolidated their predecessors' research outputs and concluded four stages of microcrack development on a concrete material under monotonic compression load. The first stage is the development of no-load bond cracks due to the cement paste's shrinkage during the hydration under the curing period, and these cracks have a trivial effect on concrete at small loads. The second stage is when the stress-strain curve of the concrete remains linear up to 30 percent of the concrete strength despite the presence of no-load bond cracks. Meanwhile, if the applied stress approach 30 to 40 percent, it will exceed the paste-aggregate interface strength, and bond cracks will form. The third stage is when the load reaches 50 to 60 percent of the ultimate strength, and localized mortar cracks will develop between the bond cracks. Furthermore, the fourth and last stage is when the load reaches 75 to 80 percent of the ultimate strength, numerous mortar cracks will develop between bond cracks, and continuous microcracks will form [27].

Shokouhi et al. [36] stated that if damage density progresses, the microcracks will eventually grow, widen, merge, and develop as macrocracks, visible damage and indicating that the concrete is at the critical level. On the other hand, if a microcrack goes undetected and becomes a macrocrack, irreversible damage, sudden failure, and major repairs are the possible consequences to the structure. It is noteworthy that when higher-order elastic constants are considered, both the acoustoelastic effect and microcracks directly affect the stress-strain behavior of concrete and ultrasonic pulse propagation [24]. Meanwhile, this research considered that microcracks affect the ultrasonic wave characteristics, such as the ultrasonic pulse velocity and pulse attenuation, as discussed by Zhang et al. [37] and Kim et al. [38]. Moreover, this research neglected the acoustoelastic effect through higher-order elastic constants and focused only on second-order elastic constants.

C. Damage Mechanics

Concrete is a heterogeneous material with numerous micro-structural discontinuities that creates a complex mechanical behavior when subjected to loading. For more than a century, an immense amount of research has been directed to develop numerical methods to model the macroscopic constitutive of concrete cracking. Damage mechanics can be classified into fracture mechanics and continuum damage mechanics. The fracture mechanics framework considers damage propagation as a discontinuous phenomenon. As a result, the concrete crack model is composed of three component parameters to capture material degradation. The first is the condition for the determination of crack initiation, the second is the methods for crack representation, and the third is the criteria that describe crack propagation [39].

Meanwhile, the continuum damage mechanics framework is based on the constitutive model of irreversible thermodynamics. Continuum damage mechanics considers damage propagation as a continuous phenomenon. A single damage parameter must be defined together with the formulation of a physical damage evolution law to capture the material degradation caused by microcrack initiation, coalescence, propagation, and stiffness reduction [40]. Moreover, in 1958 Kachanov [41] introduced continuum damage mechanics when he published a study about creep fracture. The author used a continuous variable to quantify the density of defects prior to the formation of macrocracks.

$$\phi = \frac{E}{E_0} \tag{1}$$

Where ϕ is the damage variable, E_0 is the undamaged elastic modulus, and E is the damaged elastic modulus. After more than a decade, Rabotnov [42] in 1969 introduced a complementary parameter to describe a material's damage variable that allows practical engineering applications [43].

$$D = 1 - \phi$$

$$D = 1 - \frac{E}{E_0} \tag{2}$$

Voyiadjis and Yip [44] stated that the damage variable D represents the average scalar degradation of the material in various forms, such as initiation, growth, and propagation of microcracks, cavities, and voids. Since then, numerous studies have been conducted using the damage variable. Lemaitre [45] in 1971 and Chaboche [46] in 1974 used the damage variable to study different fatigue applications. Leckie & Hayhurst [47] in 1974, Hult [48] in 1974, and Chaboche and Lemaitre [49] in 1975 use the damage variable to study creep and creep-fatigue interaction. In addition, Lemaitre and Dufailly [50] in 1977 and Lemaitre [51] in 1985 used the damage variable to study the ductile plastic fracture.

Lemaitre [52] emphasized that the scalar nature of the damage variable is sufficient to give the correct predictions for the strength capacity and the local failure of the structural component. The author added that the difficulty of modeling and calculation makes the anisotropic damage variable less reliable and requires further improvements. On the other hand, Pardoen et al. [53] present the limitation of the scalar damage parameter in predicting the mechanical degradation of a ductile material fractured by void coalescence. The author emphasized that the scalar damage parameter is best to describe damage propagation of a ductile material in two-dimensional defects like microcracks rather than three-dimensional defects like cavities since it becomes geometrically dependent on the specimen. Meanwhile, in a study, Nogueira and Willam [14] and Nogueira and Rens [4] used Lemaitre and Chaboche's damage assessment model on

plain concrete under compression and tensile stresses to monitor the propagation of mechanical damage based on elastic moduli such as the elastic modulus and shear modulus. The authors concluded that the degradation of elastic moduli follows the same rate with respect to tensile loading.

Furthermore, this research focused on continuum damage mechanics to quantify the mechanical property deterioration of reinforced concrete beams under the monotonic stress field using a damage variable as described by Equation 2, considering isotropic mechanical degradation as well as the damage assessment model proposed by Lemaitre and Chaboche [43]. In addition, the classical linearized theory of elasticity of an isotropic medium was used to express the UPV values in terms of elastic modulus for the RC beam specimens before and after the application of the monotonic stress field. Additionally, the Poison's ratio and concrete density were assumed to be constants, so the damage propagation manifested through the deviations of elastic modulus. Thus, the formula that expressed UPV reading through elastic modulus is shown in Equation 3.

$$\rho_{Conc.}(V)^2 = \frac{E(1-\upsilon)}{(1+\upsilon)(1-2\upsilon)} \tag{3}$$

Where $\rho_{Conc.}$ is the concrete density, υ is the Poison's Ratio, V is the UPV reading, specifically the longitudinal wave, and E is the elastic modulus. Meanwhile, subsequent to the RC beam's destructive test, damage propagation was measured as the degradation of damage variable, which is associated with the concrete's elastic modulus. Thus, combining Equation 2 and 3, the calculation of the scalar damage variable based on the elastic modulus was expressed using the formula:

$$D = 1 - \left(\frac{V_1}{V_0}\right)^2 \tag{4}$$

The scalar damage models were determined by creating a graph between the scalar damage parameter D and the flexural stress-strength ratio, a ratio between the ultimate stress experienced by the RC beam and the equivalent stress with respect to the corresponding value of the scalar damage variable.

Ultimately, this research was conducted to improve the sensitivity of the NDE techniques, particularly the UPV test, with the development of the scalar damage models based on the elastic modulus with respect to the applied monotonic stress. These graphs provide information about the damage patterns and propagations with respect to the RC beam's steel ratio, concrete strength, nature, and intensity of the applied stress. Furthermore, the scalar damage model detects the progression of damage at the microscopic level prior to the formation of macroscopic defects, which is commonly visible when the damage level is critical and irreversible.

II. Materials and Methods

A. Materials and Specimens

The research program used twenty-seven (27) reinforced concrete (RC) beams with their dimensions are as shown in Figure 1, where the concrete strength, steel ratio, nature, and intensity of the applied stress are the main variations. Three different concrete strengths were used, such as 3000, 4000, and 5000 Psi. In addition, the concretes are commercially available ready-mixed concrete sponsored by a private company, where the 4000 and 5000 Psi concretes are Pumpcrete Design (PCD), and the 3000 Psi is an Ordinary Design (ORD) ready-mixed concrete.

Moreover, varying amounts of 20 mm in diameter flexural deformed reinforcement bars were used with five (5) different steel ratios, such as 1.208%, 1.812%, 2.435%, 3.797%, and 5.150%, as shown in Figure 2. On the other hand, a 75 mm center-to-center fixed Stirrups spacing that varies in diameter from 10 mm to 16 mm was also used, as shown in Table 1. Furthermore, there are three different locations for the 54 kHz ultrasonic transducers that simultaneously monitored the ultrasonic pulses to capture damage propagation with respect to the intensity and nature of the applied monotonic stress, as shown in Figure 1.

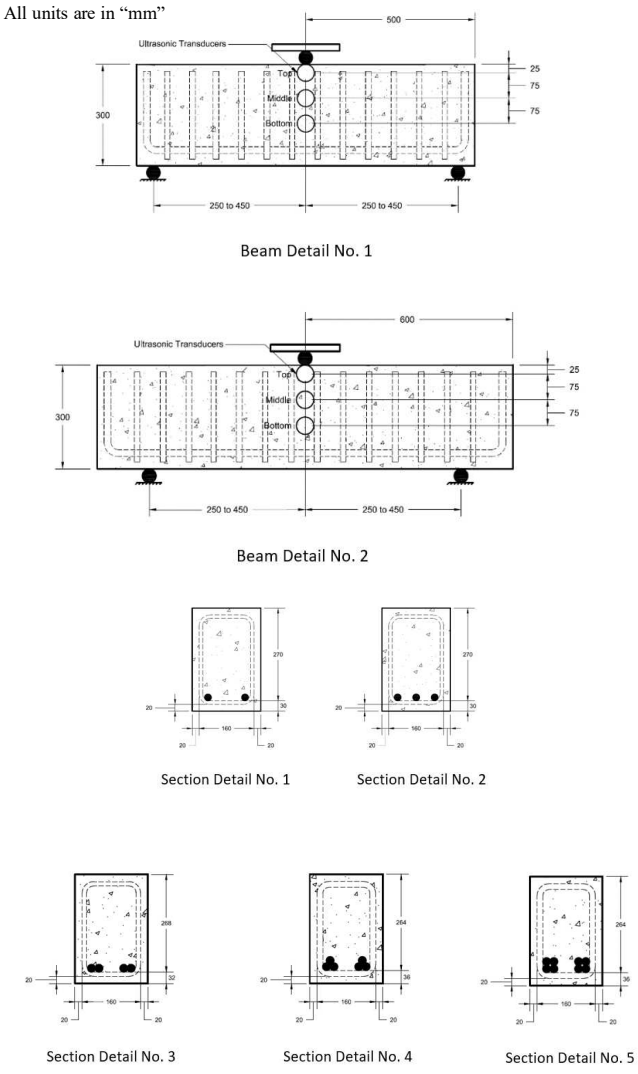

Fig. 1 Beam and Section Details

Fig. 2 Deformed Reinforcement Bars

TABLE I
DESIGN MIX PROPORTION

Mix Design	A			B			C		
Compressive Strength (MPa/Psi)	21 / 3000			28 / 4000			35 / 5000		
Design		ORD			PCD			PCD	
No. of Main Rebar (Pcs)	2	3	4	3	4	6	4	6	8
Dia. of Stirrups Rebar (mm)	10	10	12	10	12	16	12	16	16
Section Detail	1	2	3	2	3	4	3	4	5
Beam Detail	1	1	1	1	1	1	1	1	2

B. Research Instrument

The Research's UPV devices are PUNDIT Lab$^+$ with 54 kHz ultrasonic transducers, as shown in Figure 3. The PUNDIT Lab$^+$ is a flexible UPV test instrument designed primarily for laboratory operations with a measuring range of 15 m and a bandwidth of 20 to 500 kHz, and a measuring resolution of 0.1 µs. It can also be controlled remotely using PROCEQ Punditlink software that can turn computers into an oscilloscope. In addition, to the data logging function for data gathering, analysis, and export capabilities of third-party software. Meanwhile, in this research, the PROCEQ Punditlink software settings are as follows; the distances are measured from the actual concrete specimens, and the velocity is an automatic output of the UPV device derived from the input distances and transit time of the ultrasonic pulses. Moreover, both amplitude and Rx probe gain were set automatically while the time frame or the measuring resolution was set as 0.5 µs.

Consequently, for the data logging interface, the inputs are the following: reading interval was set every 1-second while the number of events was set to 5000, the device's maximum capacity. Moreover, the number of readings per event was set to 1. For the advanced settings, the probe was set as 54 kHz based on the resonating frequency of the ultrasonic transducers, while the pulse width is a default value corresponding to the selected frequency of ultrasonic transducers. Furthermore, the correction factor due to the temperature is 1.0, as recommended by the operating manual of the UPV device for surface temperature between 10 to 30 degrees Celsius. Ultimately, for the unit length and compressive strength unit, meters "m" and Megapascal "MPa" were used, respectively, while the conversion curve was neglected.

Fig. 3 PUNDIT Lab$^+$ with 54 kHz Ultrasonic Transducers

C. Research Setup

Prior to the measurement of the UPV reading in the RC beam, a functional check of the equipment and zero-time adjustments were performed to ensure that the devices were appropriately calibrated. Consequently, the RC beam was placed at the UTM on top of the fabricated flexural attachment between two steel rods. The on-center distance of steel rods ranges from 500 mm to 900 mm, with an overhang on both ends of the beam. Moreover, the 54 kHz ultrasonic transducers were placed at three specific points securely attached by the fabricated ultrasonic transducer holders to the surface of the concrete specimen. In addition, the direct transmission was used by placing the transducers directly opposite each other with petroleum jelly as the coupling agents, as shown in Figure 4.

Furthermore, the transducers were attached firmly to the RC beam's surfaces until a stable transit was displayed as prescribed by ASTM C597, which is the standard test method for pulse velocity through concrete. At the same time, since the distance between the transducers was initially determined prior to the UPV measurement and served as an input to the PROCEQ Punditlink software, the UPV reading was then automatically computed and displayed by the UPV device.

Fig. 4 Ultrasonic transducer attached to the RC beam

Once the PROCEQ Punditlink software's inputs were incorporated, the initial measurements of ultrasonic pulses began at each UPV device with a minimum of 10 readings per device with the assurance that each reading has a hundred percent transmission with no zero UPV reading included. Consequently, prior to the development of the scalar damage model, the RC beam was subjected to a destructive flexural strength test under the provisions of ASTM C293, which is the standard test method for the flexural strength of concrete using a simple beam with center-point loading. The load was then applied at the center of the RC beam while gradually increasing with a loading rate of one kN/s. Simultaneously, the UPV reading and pulse attenuation were recorded using the data logging mode of PUNDIT Lab$^+$ to the specified locations of the ultrasonic transducers as discussed earlier, until beam failure, as shown in Figure 6.

Additionally, the UTM built-in computer's analyzing software records each RC beam's load-time and load-displacement curves during the flexural strength test, as shown in Figure 5. Meanwhile, subsequent to the RC beam's destructive test, damage propagation was measured as the

degradation of the damage variable, which is associated with the concrete's elastic modulus.

Fig. 5 Flexural strength test of RC beam while simultaneously measuring the ultrasonic pulses

In addition, the scalar damage variable used in this research was determined using the variations of concrete's elastic modulus relative to the applied stress increase. Thus, the scalar damage parameter calculation based on the elastic modulus was computed using Equation 4, as discussed earlier. Moreover, the scalar damage models were determined by creating a graph between the scalar damage parameter and the flexural stress-strength ratio, a ratio between the ultimate stress experienced by the RC beam and the equivalent stress with respect to the corresponding value of the scalar damage parameter, this graph shows the mechanical damage degradation using the elastic modulus as a parameter to defined damage.

Fig. 6 Totally Damage RC beam

III. Results and Discussions

The flexural strength test for the beam specimen was conducted while simultaneously measuring the ultrasonic pulses at three different locations consistent with the research design until beam failure. The effect of stress intensity, nature of stress, steel ratio, and concrete strength was studied in relation to the scalar damage and flexural stress-strength ratio. The subsequent discussions present the relations of concrete mixture A to scalar damage, flexural stress-strength ratio, stress intensity, nature of stress, and steel ratio. Figures 7 to 9 are the scalar damage to the flexural stress-strength ratio of beam specimens with steel ratios of 1.208%, 1.812%, and 2.435%. Each graph is divided into two sets of data with its data trend as shown in the figures using linear (elastic) and nonlinear regression (rupture).

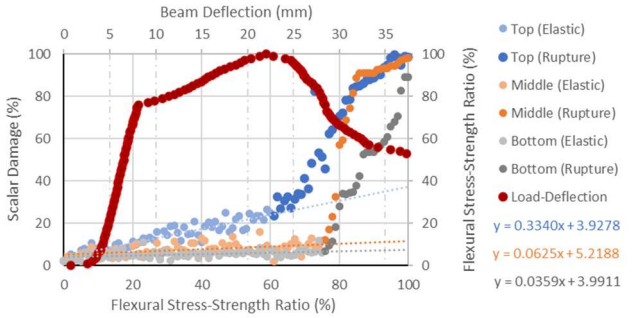

Fig. 7 Scalar Damage and Beam Deflection to Flexural Stress-Strength ratio of RC Beam (RC-S-MA-T1-0306)

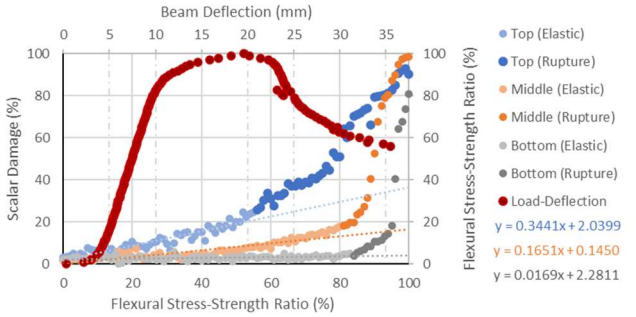

Fig. 8 Scalar Damage and Beam Deflection to Flexural Stress-Strength ratio of RC Beam (RC-S-MA-T2-0306)

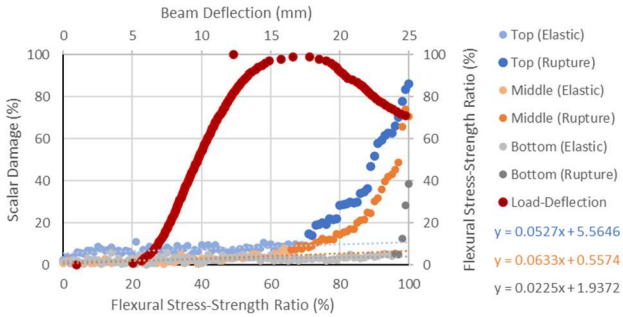

Fig. 9 Scalar Damage and Beam Deflection to Flexural Stress-Strength ratio of RC Beam (RC-S-MA-T3-0306)

The first data set is the elastic data trend since the beam deflection to flexural stress-strength ratio forms a linear relationship under these regions that signifies the general behavior of an elastic material. In addition, most of the microcracks are formed under this region, which is a significant loading stage to monitor for early damage detection. On the other hand, the second data set is the rupture data trend. At this loading phase, the UPV readings are drastically deteriorating because the beam's section is heavily damaged and under the plastic condition where successive stress redistribution occurred prior to the formation of plastic hinges. Moreover, macrocracks are formed at this stage due to microcrack accumulation that merges to form visible and irreversible damages.

Consequently, the figure's geometrical analysis, such as the inclination angle, which is pioneered by this research, was

used in the scalar damage model to monitor the early damage propagation. In addition, the inclination angle is a parameter proportional to the deviations of UPV reading as the stress level increases. Meanwhile, the scalar damage of the top transducers showed early signs of damage propagation as compared to the middle, and bottom transducers since the inclination angles of the elastic data trend in Figures 7 and 8 are 18.468° and 18.989°, respectively, which is higher compared to the middle transducers with 3.579° and 9.373°, respectively, in contrast to the bottom transducers with 2.053° and 0.968°, respectively. These gradual deviations of scalar damage represented by the inclination angle indicate microstructural degradation detected using ultrasonic pulses and further magnified by the scalar damage formula to monitor the concrete's degradation prior to the formation of macrocrack defects and aligned with the studies of Nogueira and Rens [4] and Gaviña et al. [5]. On the contrary, the middle transducers of Figure 9 showed early signs of deterioration with an inclination angle of 3.621° compared to the top transducers with 3.014°. On the other hand, this case is isolated since it happens once out of nine average samples having different concrete strengths.

Furthermore, the difference in the deviations of the scalar damage parameter showed that damage propagates at a different rate relative to the nature and intensity of the applied stress. These deviations from the initial readings are clear indications of the microstructural degradation detected by the ultrasonic pulses prior to the formation of macrocrack defects, which agrees with the observations made by Shah and Chandra [12] and Lillamand et al. [23]. Moreover, damage propagation starts at the compression part of the beam where the top ultrasonic transducers were placed, and damage propagates towards the beam's neutral axis prior to the reinforcement bar yielding. As shown in Figures 7 and 8, both Top and Middle transducers were placed under compression stress but different in stress intensities, and the result showed that top transducers with the higher stress intensity deteriorate earlier than middle transducers. In addition, the early deterioration of concrete under compression stress could be the result of a nonlinear strain distribution under the D-region. Since the proposed research setup is generally aligned with the deep beam classification as discussed by Schlaich and Schafer [54] thus, it is required to have a strut-and-tie model for the section under the discontinuity region. On the other hand, the effect of the nature of the applied stress is significantly affected by the amount of reinforcement as observed data showed that the transducers under compression stress deteriorate earlier as compared to transducers under tension since the concrete under tension stress starts to deteriorate consequent to rebar yielding as shown in the Figures 7, 8, and 9. Although the concrete under compression stress deteriorates earlier, the concrete under tension drastically deteriorates at a higher stress level after the rebar yielding, as shown in the steep slope of the bottom data series.

The drastic deteriorations captured by the scalar damage for the critical transducer based on the inclination angles were at 60%, 55%, and 65% stress levels, in agreement with the literature, such as L'Hermite [29], Rusch [30], and Sell [31]. Ultimately, the scalar damages at 100% stress levels are 89.087%, 98.386%, and 98.429% for Figure 7, together with 81.023%, 98.626%, and 90.347% for Figure 8, in contrast to 38.706%, 70.690%, and 86.225% of Figure 9, for data series Bottom, Middle, and Top, respectively. These data further reinforced the observations that the beam's section is heavily damaged and under the plastic condition where the successive stress redistribution occurred prior to the formation of plastic hinges, in agreement with the discussions of Wight and MacGregor [27].

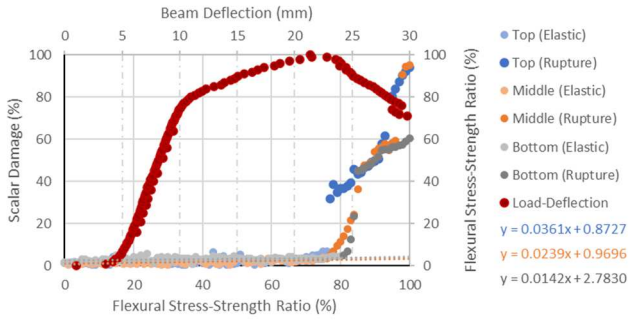

Fig. 10 Scalar Damage and Beam Deflection to Flexural Stress-Strength ratio of RC Beam (RC-S-MB-T1-0229)

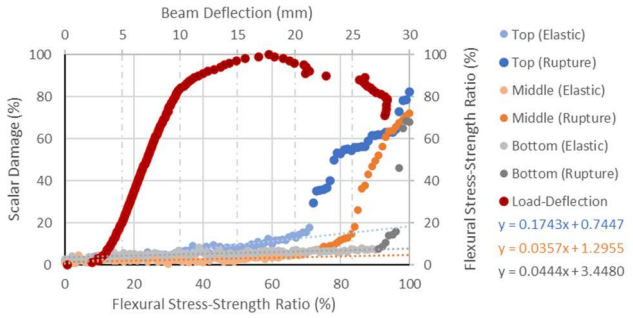

Fig. 11 Scalar Damage and Beam Deflection to Flexural Stress-Strength ratio of RC Beam (RC-S-MB-T2-0229)

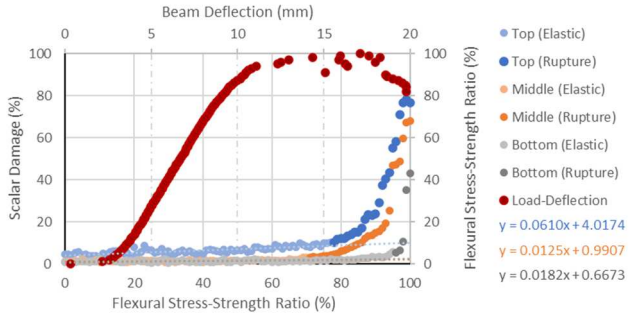

Fig. 12 Scalar Damage and Beam Deflection to Flexural Stress-Strength ratio of RC Beam (RC-S-MB-T3-0229)

Conclusively, the relationships of the steel ratio to the inclination angle of the elastic data trend are exhibited in Figures 7 to 9. Hence, as the amount of steel reinforcement increases, the inclination angle also decreases, and the additional reinforcement bar stiffened the concrete's response to tension stresses where the bottom transducers were placed. This additional stiffness is also shared for the concrete compression part where the top and middle transducers were attached. This behavior is a brittle response and critical since there is no warning prior to the sudden collapse. Furthermore,

this research reinforced the American Concrete Institute (ACI) code principles that limit the amount of steel ratio to assure the beam's ductility to the applied load.

The subsequent discussions below present the empirical relations of concrete mixture B to scalar damage, flexural stress-strength ratio, stress intensity, nature of stress, and steel ratio. Figures 10 to 12 are the scalar damage to the flexural stress-strength ratio of beam specimens with steel ratios of 1.812%, 2.435%, and 3.797%. Consistent with concrete mixture A, the scalar damage of the top transducers showed early signs of damage propagation compared to the middle and bottom transducers since the inclination angles of the elastic data trend are 2.067°, 9.888°, and 3.492°, which is higher compared to the middle transducers with 1.369°, 2.046°, and 0.717°, in contrast to the bottom transducers with 0.814°, 2.541°, and 1.044° of Figures 10, 11, and 12, respectively.

In relation, the effect of the nature of the applied stress is significantly affected by the amount of steel reinforcement; data showed that the transducers under compression stress deteriorate earlier as compared to transducers under tension since the concrete under tension stress starts to deteriorate consequence of rebar yielding as shown in Figures 10, 11, and 12. Although the concrete under compression stress deteriorates earlier, the concrete under tension drastically deteriorates at a higher stress level after the rebar yields, as shown in the steep slope of the bottom data series. Moreover, the drastic deteriorations captured by the scalar damage for the critical transducer based on the inclination angles were at 76%, 71%, and 65% stress levels. Ultimately, the scalar damage at 100% stress levels are 60.512%, 95.129%, and 94.176% for Figure 10 together with 67.939%, 72.238%, and 82.436% for Figure 11, in contrast to 42.849%, 67.874%, and 76.471% of Figures 12 for data series Bottom, Middle, and Top, respectively. Conclusively, the relationships of the steel ratio to the inclination angle of the elastic data trend are exhibited in Figures 10 to 12. Hence, as the amount of steel reinforcement increases, the inclination angle also decreases. Consistent with the discussions of concrete mixture A,

The subsequent discussions below present the empirical relations of concrete mixture C to scalar damage, flexural stress-strength ratio, stress intensity, nature of stress, and steel ratio. Figures 13 to 15 are the scalar damage to the flexural stress-strength ratio of beam specimens with steel ratios of 2.435%, 3.797%, and 5.150%. Consistent with concrete mixtures A and B, the scalar damage of the top transducers showed early signs of damage propagation compared to the middle and bottom transducers since the inclination angles of the elastic data trend are 8.036°, 7.440°, and 4.208°, which is higher compared to the middle transducers with 0.554°, 1.639°, and 0.684°. In contrast to the bottom transducers with 1.262°, 0.465°, and 1.993° for Figures 13, 14, and 15, respectively.

In relation, similar to concrete mixture A and B, the effect of the nature of the applied stress is significantly affected by the amount of steel reinforcement; data showed that the transducers under compression stress deteriorate earlier as compared to transducers under tension stress, as shown in Figures 13, 14, and 15. In effect, although the concrete under compression stress deteriorates earlier, the concrete under tension drastically deteriorates at a higher stress level after the rebar yields, as shown in the steep slope of the bottom data series. Moreover, the drastic deteriorations captured by the scalar damage for the critical transducer based on the inclination angles were at 65%, 71%, and 65% stress levels. Ultimately, the scalar damage at 100% stress levels were 37.843%, 78.838%, and 95.641% for Figure 13 together with 14.043%, 94.242%, and 95.155% for Figure 14, in contrast to 63.812%, 92.097%, and 85.534% of Figure 15 for data series Bottom, Middle, and Top, respectively.

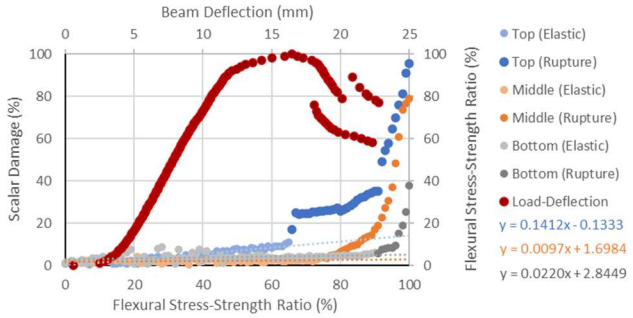

Fig. 13 Scalar Damage and Beam Deflection to Flexural Stress-Strength ratio of RC Beam (RC-S- MC-T1-0217)

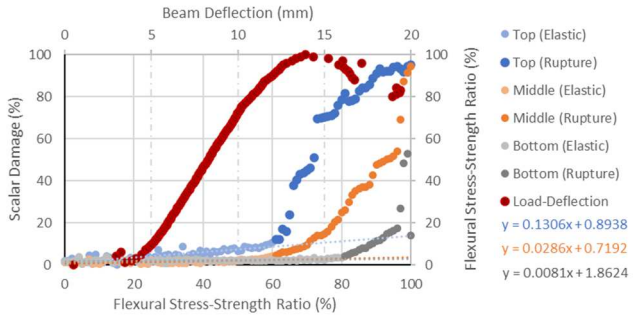

Fig. 14 Scalar Damage and Beam Deflection to Flexural Stress-Strength ratio of RC Beam (RC-S- MC-T2-0217)

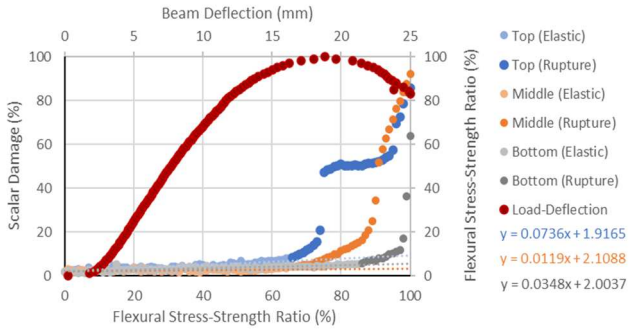

Fig. 15 Scalar Damage and Beam Deflection to Flexural Stress-Strength ratio of RC Beam (RC-S- MC-T3-0217)

Conclusively, the relationships of the steel ratio to the inclination angle of the elastic data trend are exhibited in Figures 13 to 15. Hence, as the amount of steel reinforcement increases, the inclination angle also decreases. Consistent with the discussions of pervious concrete mixtures, the additional reinforcement bar stiffened the concrete's response to tension stresses where the bottom transducers were placed.

Ultimately, the relationships of concrete strength based on the scalar damage and flexural stress-strength ratio are clearly demonstrated in Figures 8 to 14. For the concrete mixtures A and B, Figures 8 and 10 are compared with a steel ratio of 1.812%, together with the concrete mixtures A, B, and C, Figures 9, 11, and 13 are compared with a steel ratio of 2.435%. In contrast to Figures 12 and 14 of concrete mixtures, B and C are compared with a steel ratio of 3.797%. Based on the majority of these figures, the concrete strength affects the damage propagation. The higher the concrete strength, the earlier the drastic deterioration of the scalar damage variable concerning the flexural stress-strength ratio; the inclination angle also decreases. The brittle nature of concrete, having a strain limitation of 0.003, as discussed by Wight and MacGregor [27], is the reason behind this behavior. Although the beam capacity increases with the concrete strength, the strain limitation moves backward with the stress level. This indicates that concrete with higher strength develops the strain limitation at lower stress levels and vice versa.

IV. Conclusion

The intensity of the applied stress affects the inclination angle of the elastic data trend. Based on the observed data, the transducers placed at different locations exhibited different scalar damage parameter deterioration rates. The higher the applied stress intensity, the higher the inclination angle. This study established the superiority of a damage parameter based on the elastic modulus to monitor early damage propagation compared to plain UPV readings.

The nature of the applied stress affects the inclination angle of the elastic data trend. Based on the observed data, the inclination angle of concrete under compression stress is higher than concrete under tension. In addition, the scalar damage parameter at data trend's transition for transducers under tension stress drastically deteriorates at a higher stress level than transducers under compression, consequent to rebar yielding.

The amount of steel reinforcement affects the inclination angle of the elastic data trend. The additional steel reinforcement stiffened the concrete's response to tensile stresses based on the observed data, and this stiffness was also shared for the concrete under compression. The elastic data trend's inclination angle decreases as the amount of steel ratio increases.

The concrete strength affects the elastic data trend's inclination angle. In this study, it was established that the inclination angle also decreases as the concrete strength increases. The brittle nature of concrete with its strain limitation is the reason behind this behavior.

The beams with ductile response to the applied load tend to have a large inclination angle for the elastic data trend, while its UPV readings at the data trend's transition are still greater than 3000 m/s which is conventionally accepted as concrete within normal to good quality even though the beam undergoes critical stress redistribution as it approaches plastic hinging. Moreover, UPV readings exhibited consistency and sensitivity better than pulse attenuation on higher stress levels, which disagrees with the literature. Furthermore, this study showed that the scalar damage model exhibited superiority in quantitatively monitoring the early damage propagation, in contrast to UPV reading and pulse attenuation.

Acknowledgment

The authors are grateful to the administration of the Technological University of the Philippines – Manila and the Pamantasan ng Lungsod ng Valenzuela for allowing the researchers to conduct their laboratory investigations in their research centers.

References

[1] Population Division. "World Urbanization Prospects: The 2018 Revision," United Nations, New York, October 29, 2019. [Online]. Available: https://digitallibrary.un.org/record/3833745.

[2] Research Department. "World Economic Outlook: Recovery during a Pandemic—Health Concerns, Supply Disruptions, Price Pressures," International Monetary Fund, Washington, DC, October 2021. [Online]. Available: https://www.imf.org/en//Publications/WEO/Issues/2021/10/12/world-economic-outlook-october-2021.

[3] M. Rathbone, D. Chan, and O. Redrup, "Understanding Infrastructure Opportunities in ASEAN: Infrastructure Series Report 1," PwC, Singapore, 2017. [Online]. Available: https://www.pwc.com/sg/en/publications/assets/cpi-mas-1-infrastructure-opporuntities-in-asean-201709.pdf.

[4] C. L. Nogueira, and K. L. Rens, "Effect of Acoustoelasticity on Ultrasonic Pulses and Damage of Concrete under Tensile Stresses," *ACI Materials Journal*, vol. 115, no. 3, pp. 381-392, May 2018, DOI: 10.14359/51702184.

[5] J. R. Gaviña, F. A. Uy, and J. D. Carreon. (2017), Wireless Smart Sensor Network System Using SmartBridge Sensor Nodes for Structural Health Monitoring of Existing Concrete Bridges. 2nd Intl. Conf. on Civil Eng'g and Mat'l. Sci., DOI: 10.1088/1757-899X/216/1/012050.

[6] D. Balageas, C.-P. Fritzen, and A. Güemes, "Introduction to Structural Health Monitoring" in *Structural Health Monitoring*, 1st ed, London, UK, ISTE Ltd, 2006, ch 1, pp. 13-39. [Online]. Available: https://download.e-bookshelf.de/download/0000/5720/93/L-G-0000572093-0002358824.pdf.

[7] International Atomic Energy Agency, "Ultrasonic Testing," in *Guidebook on non-destructive testing of concrete structures*, 1st ed, Vienna, Austria, IAEA, 2002, ch 11, pp 100-111. [Online]. Available: https://www-pub.iaea.org/mtcd/publications/pdf/tcs-17_web.pdf.

[8] T. Powers, "Measuring Young's modulus of elasticity by means of sonic vibrations," *Proc. ASTM*, vol. 38, no. 2, pp. 460-467, 1938.

[9] R. Jones, "The Application of Ultrasonic to the Testing of Concrete," *Research London*, pp. 383-396, 1948.

[10] J. Leslie, and W. Cheesman, "An ultrasonic method of studying deterioration and cracking in concrete structures," *J. Amer. Concr. Inst.*, vol. 46, no. 1, pp. 17-36, 1949, http://refhub.elsevier.com/S0950-0618(21)00214-2/h0090.

[11] V. M. Malhotra, N. J. Carino, "The Ultrasonic Pulse Velocity Methods," in Handbook on Nondestructive Testing of Concrete, 2nd ed. Florida, USA, CRC Press, 2003, ch 8, pp. 189-205. [Online]. Available: https://vdoc.pub/documents/handbook-on-nondestructive-testing-ofconcrete-second-edition-2o6vq6n3cegg.

[12] S. Shah, and S. Chandra, "Mechanical Behavior of Concrete Examined by Ultrasonic Measurements," *Journal of Materials, JMLSA*, vol. 5, no. 3, pp. 550-563, Sept. 1970.

[13] W. Suaris, and V. Fernando, "Ultrasonic Pulse Attenuation as a Measure of Damage Growth during Cyclic Loading of Concrete," *ACI Materials Journal*, vol. 84, no. 3, pp. 185-193, Jun. 1987.

[14] C. L. Nogueira, and K. J. Willam, "Ultrasonic Testing of Damage in Concrete under Uniaxial Compression," *ACI Materials Journal*, vol. 98, no. 3, pp. 265-275, Jun. 2001, DOI: 10.14359/10282.

[15] P. Nagy, "Fatigue damage assessment by nonlinear ultrasonic characterization," *ELSEVIER, Ultrasonic*, vol. 36, no. 1-5, pp. 375-381, 1998, DOI: 10.1016/S0041-624X(97)00040-1.

[16] R. Ellwood, "The effect of microstructure and fatigue on the acoustoelastic response of aerospace materials," Ph.D. dissertation, The University of Nottingham, United Kingdom, 2012.

[17] Y. Zheng, R. G. Maev, and I. Y. Solodov, "Nonlinear acoustic applications for material characterization," *Canadian Journal of Physics*, vol. 77, pp. 927-967, 1999, DOI: 10.1139/p99-059.

[18] K.Van den Adeele, A. Sutin, J. Carmeliet, and P. Johnson, "Micro-damage diagnostics using nonlinear elastic wave spectroscopy (news)," *ELSEVIER*, NDT & E International, vol. 34, no. 4, pp. 239-248, Jun. 2001, DOI: 10.1016/S0963-8695(00)00064-5.

[19] J. Ongpeng, M. Soberano, A. Oreta, and S. Hirose, "Artificial neural network model using ultrasonic test results to predict compressive stress in concrete," *Computers and Concrete*, vol. 19, no. 1, pp. 59-68, Jan. 2017, DOI: 10.12989/CAC.2017.19.1.059.

[20] D. Y. Yoo, H. O. Shin, and Y. S. Yoon, "Ultrasonic Monitoring of Setting and Strength Development of Ultra-High-Performance Concrete," *MDPI, Materials*, vol. 9, no. 4, art. 294, Apr. 2016, DOI: 10.3390/ma9040294.

[21] M. Ju, K. Park, and H. Oh, "Estimation of Compressive Strength of High Strength Concrete Using Non-Destructive Technique and Concrete Core Strength," *MDPI, Appl. Sci.*, vol. 7, no. 12, art. 1249, Dec. 2017, DOI: 10.3390/app7121249.

[22] L. A. Camara, M. Wons, I. C.A. Esteves, and R. A. Medeiros-Junior, "Monitoring the Self-healing of Concrete from the Ultrasonic Pulse Velocity," *MDPI, J. Compos. Sci.,* vol. 3, no. 1, art. 16, Feb. 2019, DOI: 10.3390/jcs3010016.

[23] I. Lillamand, J. F. Chaix, M. A. Ploix, and V. Garnier, "Acoustoelastic effect in concrete material under uni-axial compressive loading," *Elsevier*, *NDT & E International*, vol. 43, no. 8, pp. 655–660, Nov. 2010, DOI: 10.1016/j.ndteint.2010.07.001.

[24] C. L. Nogueira, and K. L. Rens, "Acoustoelastic Response of Concrete under Uniaxial Compression," *ACI Materials Journal*, vol. 116, no. 3, pp. 21-33, May 2019, DOI: 10.14359/51714462.

[25] L. H. Chen, W. C. Chen, Y. C. Chen, H. J. Lin, C. F. Cai, M. Y. Lei, T. C. Wang, K. W. Hsu, "Using Ultrasonic Pulse and Artificial Intelligence to Investigate the Thermal-Induced Damage Characteristics of Concrete," *MDPI, Appl. Sci.*, vol. 8, no. 7, art. 1107, Jul. 2018, DOI:10.3390/app8071107.

[26] J. C. Ongpeng, A. C. Oreta, and S. Hirose, "Investigation on the Sensitivity of Ultrasonic Test Applied to Reinforced Concrete Beams Using Neural Network". *MDPI, Appl. Sci.*, vol. 8, no. 3, art. 405, Mar. 2018, DOI: 10.3390/app8030405.

[27] J. K. Wight, and J. G. Macgregor, "Materials" in Reinforced Concrete: Mechanics and Design, 6th Ed., Upper Saddle River, New Jersey: Pearson Education, Inc., 2012, http://www.civilittee-hu.com/uploads/1/RC2/book6th.pdf.

[28] F. E. Richart, A. Brantzaeg, and R. L. Brown, "A study of the failure of concrete under combined compressive stresses," University of Illinois, Eng'g Expt. Sta., bull. 185, Nov. 1928. [Online]. Available: http://hdl.handle.net/2142/4277.

[29] R. L'Hermite, "Present-day ideas on concrete technology. Part 3: The failure of concrete," RILEM, bull. 18, pp. 27-39, Jun. 1954.

[30] H. Rusch, "Physikalische Fragen der Betonpriifung," *Zement-Kalk-Gips*, vol. 12, no. 1, pp. 1-9, 1959.

[31] R. Sell, "Investigation into the strength of concrete under sustained loads," RILEM, bull. 5, pp. 5-13, 1959.

[32] T. C. Hsu, F. O. Slate, G. M. Sturman, and G. Winter, "Micro-cracking of Plain Concrete and the Shape of the Stress-Strain Curve," *ACI Journal*, vol. 60, no. 2, pp. 209-224, 1963, DOI: 10.14359/7852.

[33] F. O. Slate, and S. Olsefski, "X-Rays for the study of internal structure and microcracking of concrete," *ACI Journal*, vol. 60, no. 5, pp. 575-588, May 1963, DOI: 10.14359/7869

[34] K. Newman. "Criteria for the behavior of plain concrete under complex state of stress," In *Proc. Int. Conf. on the Struc. of Conc.: Cement and Conc. Assoc.*, London, 1968, pp. 575-588.

[35] T. T. C. Hsu, "Fatigue and Microcracking of Concrete," *Mat. Constr.*, vol. 17, pp. 51-54, Jan. 1984, DOI: 10.1007/BF02474056.

[36] P. Shokouhi, A. Zoëga, H. Wiggenhauser, and G. Fischer, "Surface Wave Velocity-Stress Relationship in Uniaxially Loaded Concrete," *ACI Materials Journal*, vol. 109, no. 2, pp. 141-148, Mar. 2012, DOI: 10.14359/51683700.

[37] Y. Zhang, O. Abraham, F. Grondin, A. Loukili, V. Tournat, A. LeDuff, and O. Durand, "Study of stress-induced velocity variation in concrete under direct tensile force and monitoring of the damage level by using thermally-compensated Coda Wave Interferometry," *Elsevier, Ultrasonics*, vol. 52, no. 8, pp. 1038-1045, Aug. 2012, DOI: 10.1016/j.ultras.2012.08.011.

[38] G. Kim, G. Loreto, J. Y. Kim, K. E. Kurtis, J. J. Wall, and L. J. Jacobs "In situ nonlinear ultrasonic technique for monitoring microcracking in concrete subjected to creep and cyclic loading," *Elsevier, Ultrasonics*, vol. 88, pp. 64-71, Aug. 2018, DOI: 10.1016/j.ultras.2018.03.006.

[39] J. Huang, M. Chen, and J. Sun, "Mesoscopic characterization and modeling of microcracking in cementitious materials by the extended finite element method," *Elsevier, Theo. and Appl. Mech. Letters*, vol. 4, no. 4, Apr. 2014, DOI: 10.1063/2.1404101.

[40] B. Wu, Z. Li, K. Tang, and K. Wang, "Microscopic Multiple Fatigue Crack Simulation and Macroscopic Damage Evolution of Concrete Beam," *MDPI, Appl. Sci.*, vol. 9, no. 21, Nov. 2019, DOI: 10.3390/app9214664

[41] L. M. Katchanov, "On the creep fracture time," In *Proc. Acad. Sci. USSR Div. Eng'g*, vol. 8, 1958, pp. 26-31.

[42] Y. N. Rabotnov and F. A. Leckie, "Creep Problems in Structural Members," John Wiley & Sons Inc., 1969.

[43] J. Lemaitre, and J. L. Chaboche, "Damage Mechanics," in *Mechanics of Solid Materials*," Cambridge, UK, Cambridge University Press, 1990, ch 7, pp. 346-450, DOI: 10.1017/CBO9781139167970.011.

[44] G. Z. Voyiadjis and S. Yip, "Continuum Damage Mechanics," In *Handbook of Materials Modeling*, 1st ed., Netherlands, Springer, 2005, ch 3, sec. 3.8, pp. 1183-1192. [Online]. Available: https://link.springer.com/chapter/10.1007/978-1-4020-3286-8_60.

[45] J. Lemaitre, "Evaluation of dissipation and damage in metals submitted to dynamic loading," *ICM*, Kyoto, Japan, 1971.

[46] J. L. Chaboche, "Une Loi Differentielle d'Endommagement de Fatigue avec Cumulation Non-Lineare," *Rev. Francaise Mecanique*, pp. 50–51, 1974.

[47] F. A. Leckie, and D. Hayhurst, "Creep rupture of structures," In *Proc. of the Royal Society*, London, UK, 1974, pp. 323-347, DOI: 10.1098/rspa.1974.0155.

[48] J. Hult, (1974). "Creep in continua and structures," In *Proc. appl. Continuum mech.*, Springer, New York, 1974, pp. 137-155.

[49] J. L. Chaboche, and J. Lemaitre, "A Nonlinear Model of creep-fatigue cumulation and interaction," In *Proc. of IUTAM, Symp. on Mech. of Viscoelastic Media and Bodies*, 1975, pp. 291-301.

[50] J. Lemaitre, and J. Dufailly, "Modelisation et Identification de l'Endommagement Plastique de Mataux," *Zeme Congres Francaise de Mecanique*, Grenoble, 1977.

[51] J. Lemaitre, "A continuous damage mechanics model for ductile fracture," *J. Eng. M. Technol.*, vol. 107, pp. 83-89, 1985.

[52] J. Lemaitre, "How to use Damage Mechanics," *Elsevier, Nuclear Engineering and Design*, vol. 80, no. 2, pp. 223-245, Jul. 1984, DOI: 10.1016/0029-5493(84)90169-9.

[53] T. Pardoen, F. Delannay, and I. Doghri, "On the use of the Lemaitre and Chaboche model for the prediction of ductile fracture by void coalescence," *Int. Journal of Fracture*, vol. 88, no. 4, pp. 71-76, 1998.

[54] J. Schlaich, and K. Schafer, "Design and detailing of structural concrete using strut-and-tie models," *The Structural Engineer*, vol 69, no.6, pp. 113-125, Mar. 1991. [Online]. Available: http://www.ime.eb.br/~webde2/prof/ethomaz/bloco_sobre_estacas/biela_tirante.pdf.